



HAL
open science

Non-Destructive Study of Egyptian Emeralds Preserved in the Collection of the Museum of the Ecole des Mines

Maria Nikopoulou, Stefanos Karampelas, Éloïse Gaillou, Ugo Hennebois, Farida Maouche, Annabelle Herreweghe, Lambrini Papadopoulou, Vasilios Melfos, Nikolaos Kantiranis, Didier Nectoux, et al.

► To cite this version:

Maria Nikopoulou, Stefanos Karampelas, Éloïse Gaillou, Ugo Hennebois, Farida Maouche, et al.. Non-Destructive Study of Egyptian Emeralds Preserved in the Collection of the Museum of the Ecole des Mines. *Minerals*, 2023, 13 (2), pp.158. 10.3390/min13020158 . hal-04246143

HAL Id: hal-04246143

<https://minesparis-psl.hal.science/hal-04246143>

Submitted on 17 Oct 2023

HAL is a multi-disciplinary open access archive for the deposit and dissemination of scientific research documents, whether they are published or not. The documents may come from teaching and research institutions in France or abroad, or from public or private research centers.

L'archive ouverte pluridisciplinaire **HAL**, est destinée au dépôt et à la diffusion de documents scientifiques de niveau recherche, publiés ou non, émanant des établissements d'enseignement et de recherche français ou étrangers, des laboratoires publics ou privés.



Distributed under a Creative Commons Attribution 4.0 International License

Article

Non-Destructive Study of Egyptian Emeralds Preserved in the Collection of the Museum of the Ecole des Mines

Maria Nikopoulou ^{1,*}, Stefanos Karampelas ^{2,*}, Eloïse Gaillou ^{3,*}, Ugo Hennebois ², Farida Maouche ³, Annabelle Herreweghe ², Lambrini Papadopoulou ¹, Vasilios Melfos ¹, Nikolaos Kantiranis ¹, Didier Nectoux ³ and Aurélien Delaunay ²

¹ Department of Mineralogy-Petrology-Economic Geology, School of Geology, Aristotle University of Thessaloniki, 54124 Thessaloniki, Greece

² Laboratoire Français de Gemmologie (LFG), 30 rue de la Victoire, 75009 Paris, France

³ Mineralogy Museum, Mines Paris, PSL University, 75006 Paris, France

* Correspondence: marthonik@geo.auth.gr (M.N.); s.karampelas@lfg.paris (S.K.); eloise.gaillou@mines-paristech.fr (E.G.)

Abstract: In the present study, rough emerald single crystals and rough emeralds in the host rock from the ruins of Alexandria and from the Mount Zabargad in Egypt, preserved in the collection of the museum of the Ecole des Mines (Mines Paris—PSL) since the late 19th or early 20th century, are investigated. All samples were characterized by non-destructive spectroscopic and chemical methods during a week-long loan to the LFG. Raman, FTIR and UV-Vis-NIR spectroscopy revealed that Egyptian emeralds contain H₂O molecules accompanied by relatively high concentrations of alkali ions and are colored by chromium and iron. Additionally, EDXRF showed that the emeralds from Egypt contain up to 84 ppm Rb and low amounts (below 200 ppm) of Cs. Inclusions and parts of the host rock were also observed under optical microscope and analyzed with Raman spectroscopy. Tube-like structures, quartz, calcite, dolomite, albite and phlogopite are associated minerals, and inclusions are identified in these historic emeralds from Egypt. This work will hopefully further contribute to the characterization of emeralds of archaeological significance.

Keywords: emeralds; beryl; Egypt; EDXRF; FTIR; Raman spectroscopy; PL; UV-Vis-NIR



Citation: Nikopoulou, M.; Karampelas, S.; Gaillou, E.; Hennebois, U.; Maouche, F.; Herreweghe, A.; Papadopoulou, L.; Melfos, V.; Kantiranis, N.; Nectoux, D.; et al. Non-Destructive Study of Egyptian Emeralds Preserved in the Collection of the Museum of the Ecole des Mines. *Minerals* **2023**, *13*, 158. <https://doi.org/10.3390/min13020158>

Academic Editor: Yamirka Rojas-Agramonte

Received: 16 December 2022

Revised: 11 January 2023

Accepted: 17 January 2023

Published: 21 January 2023



Copyright: © 2023 by the authors. Licensee MDPI, Basel, Switzerland. This article is an open access article distributed under the terms and conditions of the Creative Commons Attribution (CC BY) license (<https://creativecommons.org/licenses/by/4.0/>).

1. Introduction

Emerald is the bluish-green to green to yellowish-green variety of beryl (with an ideal formula of Be₃Al₂SiO₁₈) colored by chromium and/or vanadium (iron may also contribute to the color); beryl colored solely by iron is classified as green beryl (and not emerald) [1–3]. Emeralds are found in almost all continents but today, the most popular and commercial deposits occur in: Colombia, Zambia and Brazil, with lesser quantities found in Afghanistan, Ethiopia, Madagascar, Russia and Zimbabwe [1–3]. Emerald as a mineral is crystalized in the hexagonal crystal system and is, therefore, birefringent. This means that when light penetrates the crystal (perpendicular to c-axis), it is separated in two rays with different refractive indexes (RIs). The ordinary ray (ω -ray) and the extraordinary ray (e -ray) are $n_{\omega} = 1.5705$ – 1.5905 and $n_e = 1.5656$ – 1.5975 , respectively [4].

The crystal structure of an emerald consists of Be/Si sites surrounded by four atoms of O in tetrahedral coordination and the Al site (known as Y site) surrounded by six O atoms in octahedral coordination [1]. The SiO₄ tetrahedra form six-membered rings parallel to the c-axis (Figure 1a,b). These rings are arranged on top of each other. Viewing a beryl's crystal lattice parallel to c-axis, vacant spaces can be observed, which are called “channels”. The studies of beryl crystals with Fourier transform infrared (FTIR) spectroscopy [5] proved that water molecules can be found in the crystal's structure. Water molecules can be classified into two different types (Figure 2): Type I water molecules occur individually in the channels and the symmetry axis is positioned perpendicular to c-axis of the crystal.

Type II water molecules are accompanied by nearby alkali ions (principally Na) in the channels with the water molecule axis parallel to c-axis [6]. Sometimes, the substitution of Al in Y sites [7] with chromophore ions (for example Fe, Cr and V) is responsible for the different variety of colors in beryl. In the case of emerald, the green color is due to the substitution of Al^{3+} with Cr^{3+} and V^{3+} ions, with Fe^{3+} and Fe^{2+} contributing.

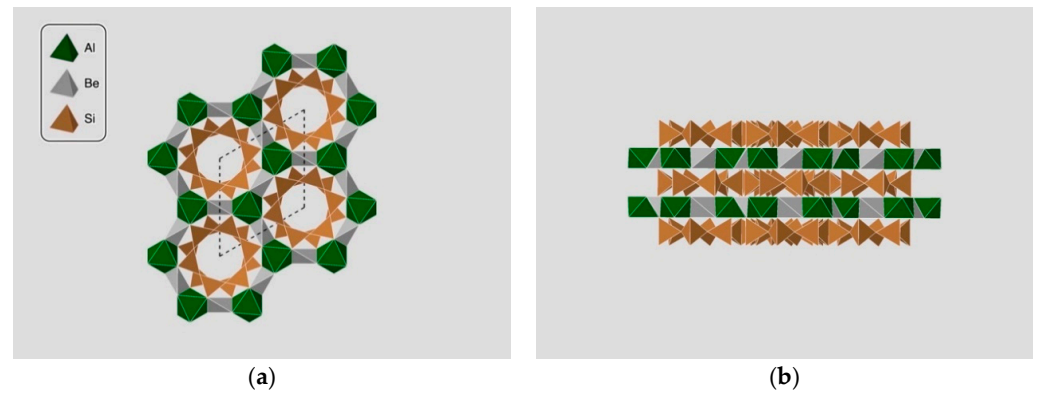


Figure 1. Crystal structure of beryl perpendicular (a) and parallel (b) to c-axis. Empty channels are mentioned with black dashed line (designed in Crystal Maker).

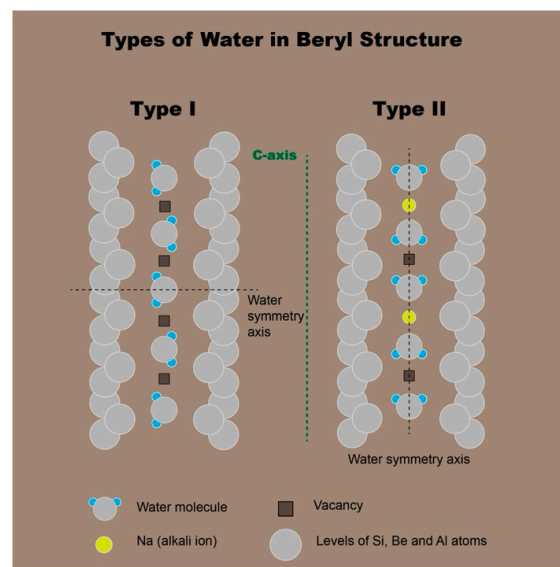


Figure 2. Type I and Type II water molecules in the channels of beryl's structure (Updated from Wood and Nassau, 1968 [5]. Designed in Adobe Illustrator).

The term “Egyptian emeralds” is associated with the legendary and historic emerald source known as “Cleopatra Mines”, a term that is used as a marketing tool [8]. The mining of emeralds began in the Wadi Sikait area in Eastern desert of Egypt [9] toward the end of the 1st century BC but most of the mining activity occurred during Roman times [1]. Today, no mining of emeralds occurs in Egypt. The last mining operations were carried out unsuccessfully in the 1920s [10]. The genesis of Egyptian emeralds is linked to the geological history of the southern Eastern Desert. According to references [11], there are at least three generations of beryl in Egyptian emerald deposits. The crystals of the first generation are colorless without zoning and show micro- and macro-cracks produced by brittle deformation. The first-generation crystals are surrounded by a second generation overgrown layer [11]. The beryl crystals in this layer have a light green color with various solid inclusions of mica, phlogopite, albite and quartz. The latest generation of beryl is a Cr-rich emerald with a deep green color and it rarely occurs in quartz veins and aplitic

dikes [11]. The edges of this generation have no cracks [11]. Significant deposits of Egyptian emeralds are in Zabara, Wadi Nugrus and Umm Kabu areas with similar geological settings, also known as Eastern Desert deposits in Egypt. Most the beryl crystals in these deposits are of the Proterozoic age and can be categorized into two paragenetic types [12]: (1) emeralds in mica-schists and (2) beryl in granitoids.

The Zabara Mountain has been known for its emerald deposits since the antiquity. In this area, emerald and beryl crystals are found in the contact between gneissic granites or meta-pegmatites (rich in quartz and feldspar) and various types of schists (rich in mica, amphiboles and talc). The granites are S-type [13] and were probably formed by the partial melting of the crust (mainly by metasedimentary rocks). The schists probably originated from the metamorphism of ophiolitic and volcanic rocks. The host rocks of beryl contain abundant fractures and joints filled by quartz veins. Additionally, many fractures in beryl crystals contain quartz. This indicates that the emeralds were crystallized first, followed by quartz. In some places, the deformation caused by later tectonic events resulted in boudinaged metapegmatoid veins in the biotite schists [14]. In the Zabara area, the emerald crystals are plentiful and large (reaching a few cm across), and their colors vary from pale greenish to deep green or bluish-green [15]. Most of the best quality emeralds are restricted to the mica rocks, close to the quartz veins.

The Wadi Nugrus area is mainly occupied by mafic and ultramafic rocks (serpentinites, metagabbros and hornblende schists), which contain garnets in places. The intrusion of a Be-enriched magma accompanied by the injection of numerous aplitic and quartz veins in ophiolites and volcanic arc rocks of the Nugrus-Ghadir constitutes the first stage of the geological history of Egyptian emeralds [11]. Most of these rocks have been metasomatized and deformed by later hydrothermal fluids and subsequent metamorphic and tectonic events. Shear zones with a NW–SE direction led to the formation of mylonites and cataclastites [12]. The emeralds are found between metasediments or various schists in contact with granitic and pegmatite intrusions. Some quartz veins and emerald-bearing schists could be associated with post-magmatic fluids and Na-metasomatism (albitization). All these processes contributed to the final formation of beryl in this region. Most emeralds in Wadi Nugrus reach a few cm across (average 3 cm) the oriented parallel to their prismatic facets [12].

The geology of the Kabu-Um Debaa area is very similar to Wadi Nugrus [10]. Rocks of this region include mica and hornblende schists and serpentinites with garnetiferous magmatic intrusions. The beryliferous zones are found close to quartz veins in contact with mica schists. According to Hassan and El-Shatouri [15], no exposures of the metasedimentary rocks were observed in this area. However, some blocks of the psammitic gneiss are observed in the mine dumps, indicating the presence of this rock at shallow depth.

2. Materials and Methods

For this study, the Ecole des Mines (Paris School of Mines-PSL) provided a short-term loan (one week), for scientific purposes, of 8 emerald samples from Egypt to the Laboratoire Français de Gemmologie (LFG) to analyze them using strictly non-destructive methods. The samples and their dimensions are listed in Table 1, as well as Figures 3 and 4. Four of these samples are single crystals (Figure 3), with a characteristic hexagonal prism shape, donated by Émile Bertrand (1844–1909) to the Ecole des Mines. According to the museum records, they come from the ruins of Alexandria [16]. These single crystal samples were also examined with classic gemological tools. The other four samples are incorporated in the host rock (Figure 4). According to the museum references, these samples were given to the museum at the end of the 19th century or at the very beginning of the 20th century. Three of them were provided by the Marquis de Raincourt (1835–1917) and one by Frédéric Cailliaud (1787–1869). Cailliaud was the leader of campaigns in the Zabara area, meaning they searched for the mythic emerald deposits in Egypt, at the beginning of the 19th century [17]. It is more than likely that sample ENSMP 47849a27 comes from one of the expeditions led by Cailliaud.

Table 1. Properties of Egyptian emeralds from Ecole des Mines.

No.	Donor's Name	Wt. (Ct.)	Dimensions (mm)	Density	Color	Shape	Observations
ENSMP 72466_01	Emile Bertrand	1.002	7.25 × 3.73 × 4.33	2.71	Vivid green	Rough	Translucent RI: 1.57-1.58 LWUV-SWUV: Inert
ENSMP 72466_02	Emile Bertrand	2.038	7.29 × 5.43 × 5.55	2.63	Vivid green	Rough	Translucent LWUV-SWUV: Inert
ENSMP 72466_03	Emile Bertrand	3.154	9.94 × 5.69 × 7.38	2.71	Vivid bluish-green	Rough	Translucent LWUV-SWUV: Inert
ENSMP 72466_04	Emile Bertrand	5.392	10 × 7.98 × 8.32	2.77	Vivid bluish-green	Rough	Translucent RI: 1.58 LWUV-SWUV: Inert
ENSMP 47849a26	Marquis de Raincourt	-	34.66 × 29.23 × 30.76	-	Vivid green crystals	Crystals in host rock	Translucent LWUV-SWUV: Inert
ENSMP 47849a27	Frédéric Cailliaud	-	25.93 × 22.74 × 24.52	-	Vivid green crystals	Crystals in host rock	Translucent LWUV-SWUV: Inert
ENSMP 72486	Marquis de Raincourt	-	31.83 × 16.83 × 21.50	-	Vivid bluish-green crystals	Crystals in host rock	Translucent LWUV-SWUV: Inert
ENSMP 13512_5	Marquis de Raincourt	-	85.6 × 57.53 × 50.08	-	Vivid bluish-green crystals	Crystals in host rock	Translucent LWUV-SWUV: Inert



Figure 3. (a,b) Macroscopic images of Egyptian single-crystal emeralds from Ecole des Mines. (b1) ENSMP 72466_01, (b2) ENSMP 72466_03, (b3) ENSMP 72466_02, (b4) ENSMP 72466_04. Photos: Eloïse Gaillou; © Musée de Minéralogie Mines Paris—PSL/E. Gaillou.

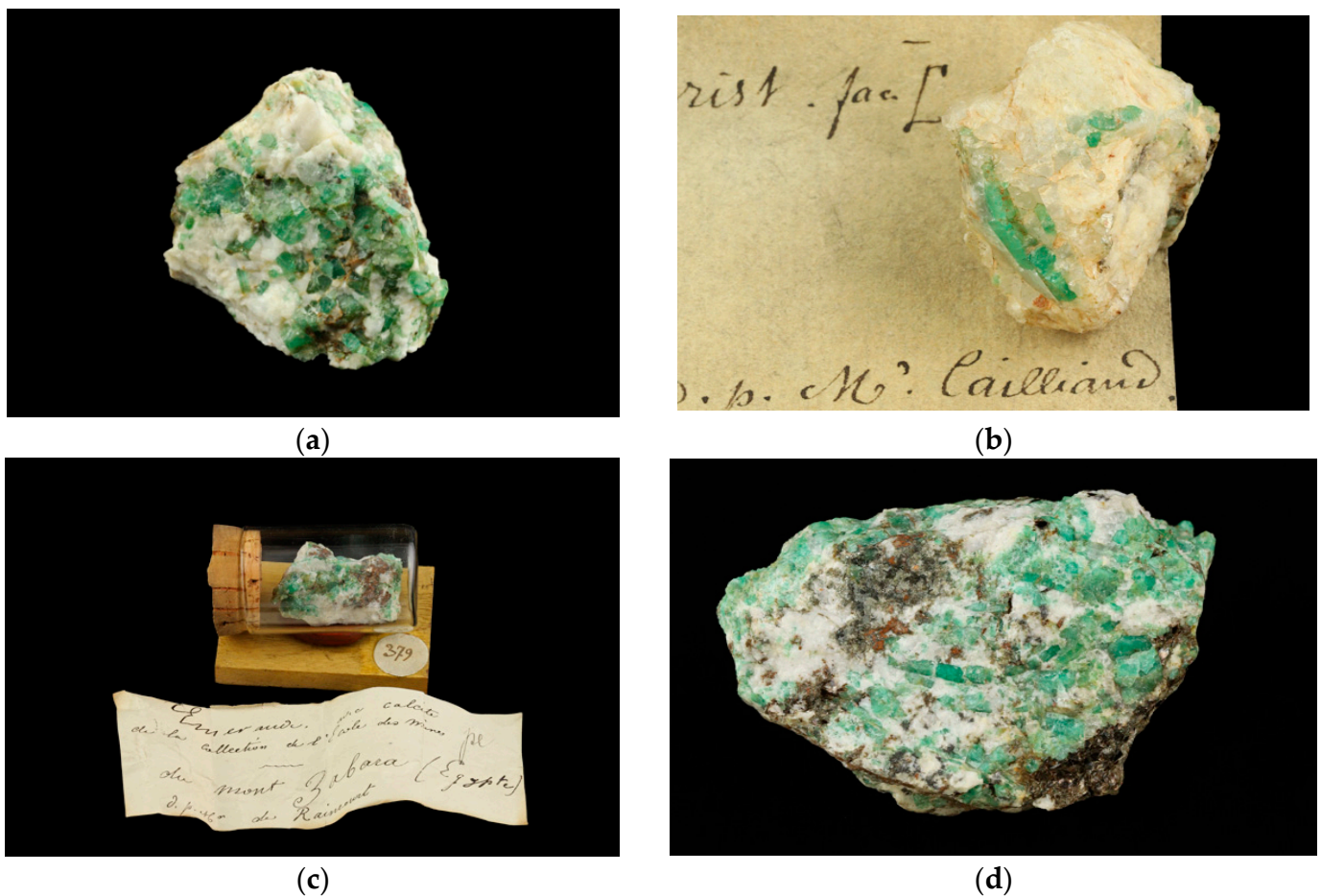


Figure 4. Macroscopic images of emerald samples included in the host rock from Ecole des Mines. (a) ENSMP 47849a26 (34.66 × 29.23 × 30.76 mm), (b) ENSMP 47849a27 (25.93 × 22.74 × 24.52 mm), (c) ENSMP 72,486 (31.83 × 16.83 × 21.50 mm), (d) ENSMP 13512_5 (85.6 × 57.53 × 50.08 mm). Photos: Eloïse Gaillou; © Musée de Minéralogie Mines Paris—PSL/E. Gaillou.

All samples were examined under a Zeiss Stemi 508 binocular microscope. Refractive index for ENSMP 72466_01 and ENSMP 72466_04 samples is measured by using a refractometer and the distant vision method (also known as spot reading). Hydrostatic balance was used to measure the density of the four samples in Figure 3. Additionally, luminescence reaction was observed for the same four samples under a 6 W ultraviolet (UV) lamp (Vilber Lourmat VL-6.LC) with long-wave ultraviolet (365 nm) and short-wave ultraviolet (254 nm) light, equipped with a CN-6 dark room (10 cm distance between the sample and the lamp).

Raman and photoluminescence (PL) spectra were acquired on the four single crystals, using mobile Raman Spectrometer (GemmoRaman-532SG, Magilabs Oy (Ltd.), Helsinki, Finland) with a 532 nm laser excitation ranging for Raman spectra from 200 to 2000 cm^{-1} (with 1 s exposure time and 4 accumulations) and for PL spectra from 540 to 760 nm (0.3 to 0.4 s exposure time and 30 accumulations). Spectra using micro-Raman Renishaw inVia spectrometer (Renishaw plc, Wotton-under-Edge, Gloucestershire, UK), coupled with an optical microscope and with a 514 nm laser excitation (diode-pumped solid-state laser) from 100 to 1500 cm^{-1} region, were obtained with 10 accumulations and 30 s of exposure time. Laser power on the sample was 40 mW for these spectra and the spectral resolution about 2 cm^{-1} . Raman spectra, for the region 3000–3700 cm^{-1} , were obtained with 20 accumulations and 15 s exposure time. Raman spectra on the associated minerals on the four rocks were acquired from 100 to 4000 cm^{-1} , with 1 accumulation and 20 s exposure time. For the PL spectra (500–900 nm), 10 s of exposure time and 1 accumulation with 0.04 mW laser power were used on the sample. A diamond was used for the calibration of both Raman spectrometers by considering its 1331.8 cm^{-1} Raman peak.

FTIR spectra (400–8000 cm^{-1}) were obtained using Nicolet iS5 spectrometer (Thermo Fischer Scientific, Waltham, MA, USA) with 4 cm^{-1} resolution and 500 scans. Visible-near infrared (Vis-NIR) spectra were acquired on the four single crystals from 365 to 1000 nm using a mobile instrument (0.05 to 0.10 s acquisition time and 50 accumulations) with an integrating sphere (Gemmosphere, Magilabs Oy (Ltd.), Helsinki, Finland). Ultraviolet-visible (UV-Vis) spectra were conducted by a Jasco V-630 from 250 to 850 nm, with a data interval (DI) and spectral bandwidth (SBW) of 2 nm and 210 nm/min scan rate. When possible, spectra were acquired parallel and perpendicular to the c-axis (for the single crystals) on the flattest parts of each stone. Due to their size, the rocks and their associated minerals were only studied by using a micro-Raman spectrometer.

For chemical analysis with EDXRF (energy dispersive X-ray fluorescence), sample holders with an aperture of 5 mm diameter were used and specific sets of parameters were optimized for the most accurate analysis of beryl. Various conditions were used for filters and voltage (no filter/4 kV, cellulose/8 kV, aluminum/12 kV, thin palladium/16 kV, medium palladium/20 kV, thick palladium/28 kV, and thick copper/50 kV), with an acquisition time of about 20 min for each sample. All measured iron was calculated as FeO.

3. Results

3.1. Macroscopic, Microscopic and Gemological Observations

The emerald samples are translucent and have a hexagonal prism habit with a vivid bluish-green to vivid green color. Interference colors are due to fissures, as well as various fractures on the surface of the crystals. Emeralds' size ranges from 2 mm to 2 cm and sometimes their growth is interrupted by the intrusion of quartz (identified by micro-Raman spectroscopy; see below) veins (Figure 5a,b). These intrusions may have taken place after the crystallization of the emeralds. Furthermore, some samples (ENSMP 1352_5) reveal boudinage tectonic structures (Figure 4d), which comes in terms with Grundmann and Morteani [14] descriptions. According to their gemological observations, emeralds of Egypt are translucent with RI that ranges from 1.57 to 1.58. All samples are inert under SWUV and LWUV, and their density varies from 2.63 to 2.77.

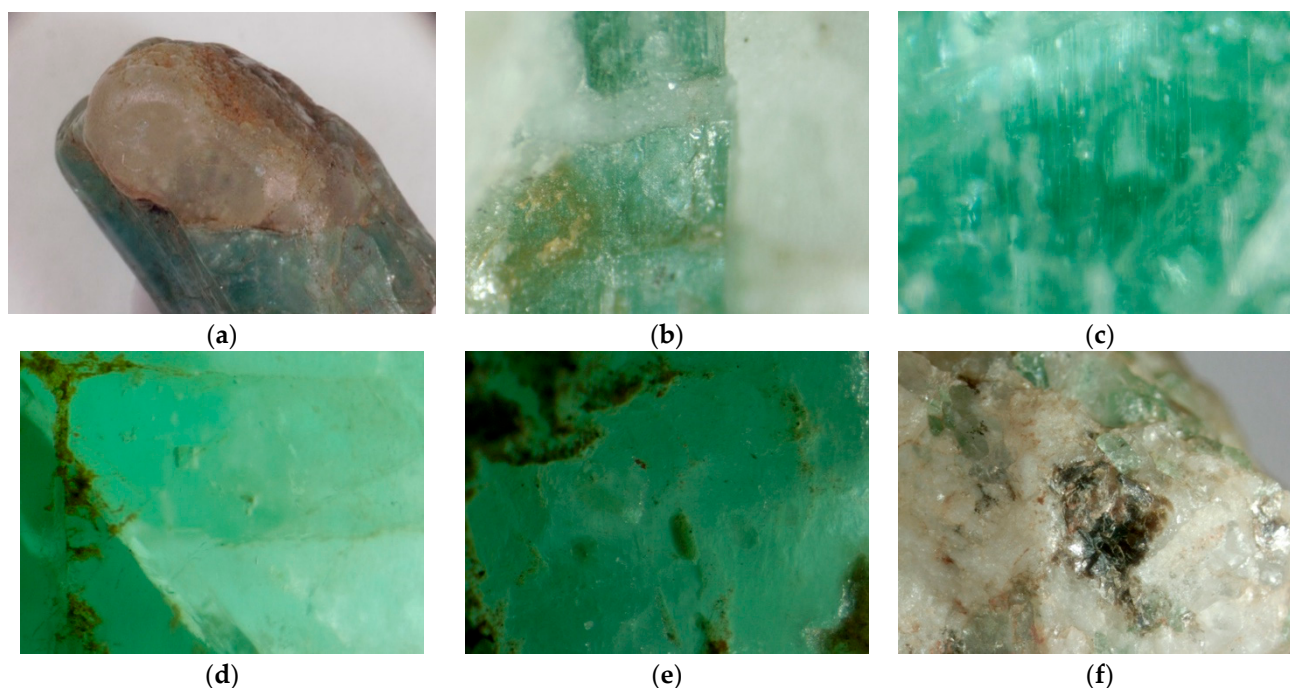


Figure 5. Macroscopic and microscopic characteristics of emeralds from Egypt. (a) Quartz crystal which interrupts the growth of an emerald crystal (ENSMP 72466_03); FOV: 8 mm, (b) Quartz vein which interrupts the growth of an emerald crystal (ENSMP 47849a26); FOV: 2 mm, (c) Growth tubes and rectangular shaped multiphase inclusions parallel to the c-axis (ENSMP 13512_5); FOV: 1 mm, (d) Rectangular crystal inclusion in an emerald crystal (ENSMP 72466_02); FOV: 1 mm, (e) Macroprismatic crystal inclusion of mica in an emerald crystal (ENSMP 72466_04); FOV: 1 mm, (f) Mica, quartz and plagioclase in the host rock of Egyptian emeralds (ENSMP 47849a27); FOV: 4 mm. Microphotos by Ugo Hennebois/LFG; © Musée de Minéralogie Mines Paris—PSL.

Under the microscope, some samples show growth tubes and rectangular shaped multiphase fluid inclusions [17,18] (Figure 5c) along with quartz and mica crystals (identified by micro-Raman spectroscopy; see below). In addition, unidentified single crystal inclusions can be observed with angular or prismatic shapes (Figure 5d) or mica inclusions in macroprismatic shapes (Figure 5e). The minerals of the host rock (Figure 5f), which are observed under the microscope, are: quartz, feldspar (possibly plagioclase) and mica (possibly phlogopite), identified by micro-Raman spectroscopy (see below).

3.2. Raman Spectroscopy

Micro-Raman technique was applied in various ranges: from 200 to 1300 cm^{-1} (Figure 6a,c) and from 3500 to 3700 cm^{-1} (Figure 6b,d). A band at around 686 cm^{-1} is observed due Be-O stretching, at around 1069 cm^{-1} it is linked with Si-O and/or Be-O stretching [3,19–23] and at around 1010 cm^{-1} and above 1100 cm^{-1} it may also be observed on natural emeralds [21] and correspond to stretching vibrations of Si-O and inner vibrations, respectively [3,20–22,24]. Raman bands between 200 and 600 cm^{-1} are related to Si_6O_{18} ring vibrations [3,20,21]. The relative intensity of the Raman bands changes with the change in spectra orientation. Alkali content can be estimated with the full width half maximum (FWHM) of the band at 1069 cm^{-1} ; all studied samples demonstrated high alkali content (Table 2) as they have a FWHM > 22 cm^{-1} , ranging from 23 to 27 cm^{-1} , while samples with medium-to-low alkali content have a FWHM < 22 cm^{-1} in the 1069 cm^{-1} band [3,20,25].

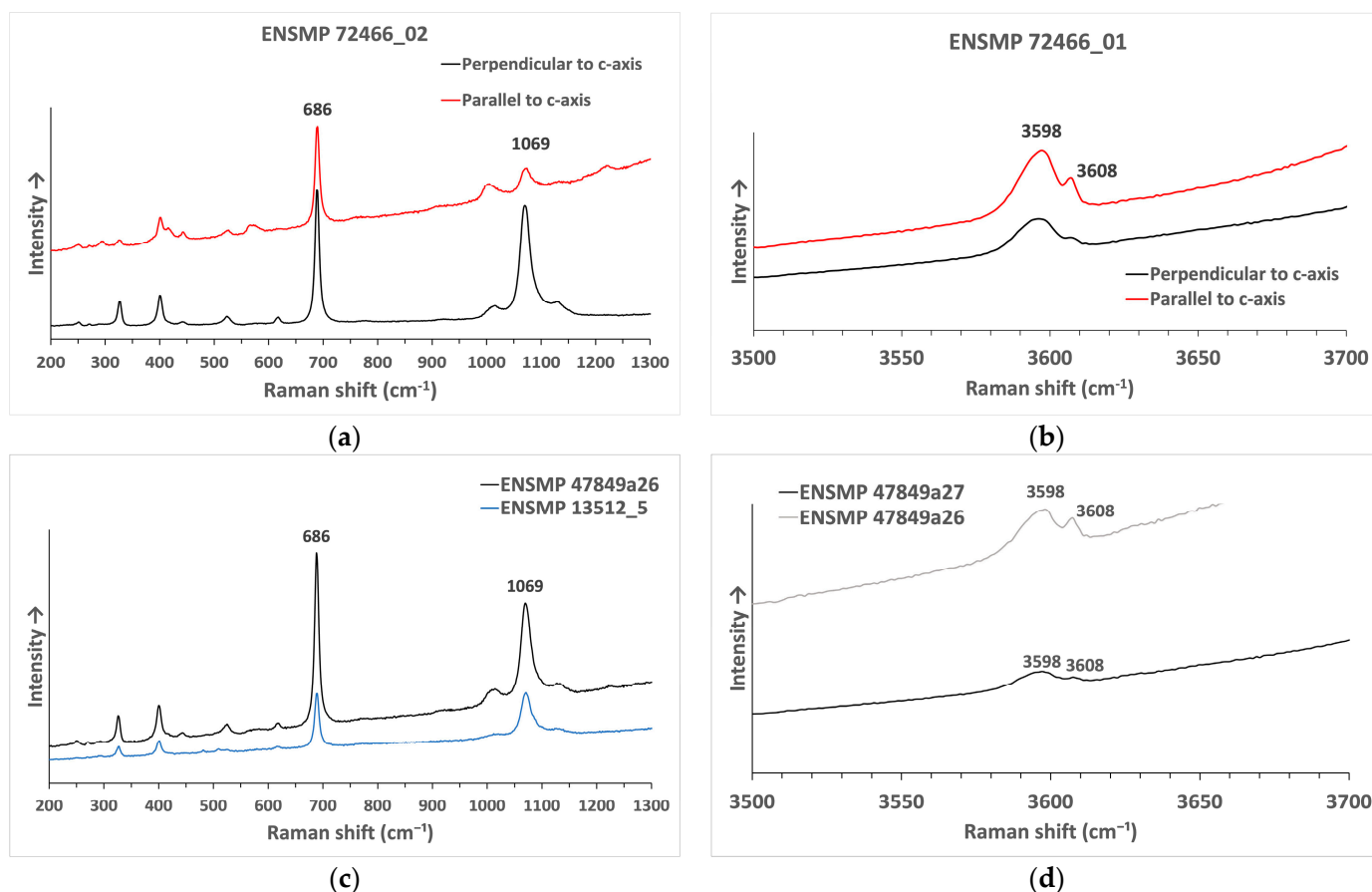


Figure 6. Micro-Raman spectra from Egyptian emeralds (using 514 laser excitation). (a) Raman spectra from 200 to 1300 cm^{-1} of a single-crystal emerald (ENSMP 72466_02) parallel (red line) and perpendicular (black line) to c-axis. Characteristic peaks at 686 and 1069 cm^{-1} are observed, while the 1069 cm^{-1} peak is more intensely parallel to c-axis. (b) Raman spectra from 3500 to 3700 cm^{-1} of a single-crystal emerald (ENSMP 72466_01) parallel (red line) and perpendicular (black line) to c-axis. Peak close to 3608 cm^{-1} is related with Type I water molecule structure. More intense bands at 3598 cm^{-1} are due to Type II water molecule structure with an alkali ion nearby. (c) Raman spectra from 200 to 1300 cm^{-1} of emeralds from samples that are included in the host rock. Spectra were acquired with the laser beam perpendicular to the prism facets. (d) Raman spectra from 3500 to 3700 cm^{-1} of the samples ENSMP 47849a27 (black line) and ENSMP 47840a26 (grey line). The intense band at 3598 cm^{-1} is related with Type II water molecules with an alkali ion nearby.

Table 2. Position and FWHM of the Raman band at around 1069 cm^{-1} , relative intensities of the Raman bands at 3598 cm^{-1} and 3608 cm^{-1} and position of the R1 photoluminescence bands for the samples of different localities. All observations were made using spectra acquired with a laser beam parallel and/or perpendicular to c-axis.

Sample No.	FWHM of Band 1069 cm^{-1}	R1/Rn
ENSMP 72466_01	24.5	0.41
ENSMP 72466_02	27	0.43
ENSMP 72466_03	26	0.35
ENSMP 72466_04	24.5	0.43
ENSMP 13512_5	24.5	0.45
ENSMP 47849a26	23	0.51
ENSMP 47849a27	24.5	0.43
ENSMP 72486	23.5	0.36

Raman spectra area from 3500 to 3700 cm^{-1} also indicates the presence or absence of alkali ions in the crystal lattice based on the height ratio of the two sharp bands situated at around 3600 cm^{-1} [3,6,23,24]. The peak around 3598 cm^{-1} is attributed to water Type II molecules vibrations (with an alkali ion nearby), and the band around 3608 cm^{-1} is attributed to water Type I molecule vibrations (without an alkali ion nearby) [20]. The higher intensity of 3598 cm^{-1} compared to 3608 cm^{-1} in all studied samples further confirms the presence of alkalis in relatively high concentrations [3,6,22,23].

Raman spectra were acquired with a mobile instrument on the following samples: ENSMP 72466_01, ENSMP 72466_02, ENSMP 72466_03 and ENSMP 72466_04. Only the main Raman bands of beryl at 686 cm^{-1} and 1069 cm^{-1} were observed with different relative intensities due to different crystallographic orientations (Figure 7) [19]. Emerald is a mineral that presents strong luminescence phenomena above 2000 cm^{-1} due to the presence of chromium.

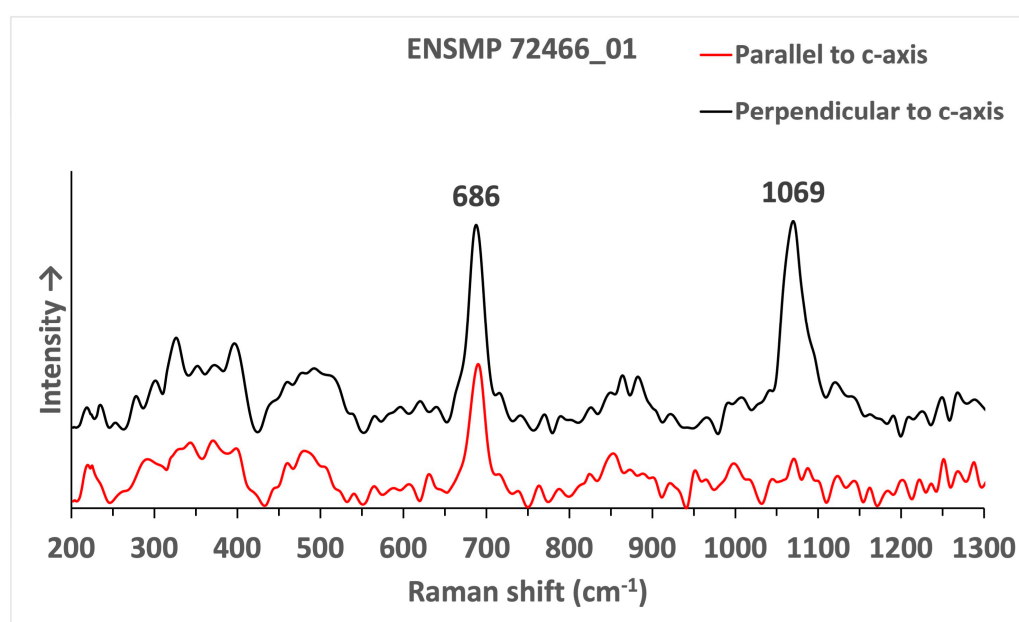


Figure 7. Raman spectra (ENSMP 72466_01) obtained using a mobile instrument with 532 nm laser excitation in the range of 200 to 1300 cm^{-1} parallel (red line) and perpendicular (black line) to the c-axis. The upper spectrum has been vertically offset for better clarity. Characteristic bands at 686 and 1069 cm^{-1} are mentioned. The Raman spectra were baseline corrected.

3.3. PL Spectroscopy

In Figure 8, PL spectra from 650 to 850 nm (Figure 8) are presented. All samples revealed two sharp peaks at around 680 and 684 nm due to Cr^{3+} (known as R2 and R1 lines, respectively), and a broad band centered at around 720–740 nm (known as Rn), which is also linked with traces of chromium [3,26]. The position of R1 band could help to separate natural from synthetic emeralds as there are no synthetic emeralds with R1 > 683.7 nm [3]. Additionally, according to Thompson et al. [27], the relative height ratio of the peaks can help in the determination of high or low concentrations of alkali ions (Table 2). In our study, the height ratio of the R1/Rn ranges between 0.36 and 0.51, revealing that the Egyptian emeralds contain relatively high alkalis while the R1 peak position is above 684 nm in all studied samples. Spectra with the mobile instruments reveal bands at similar positions.

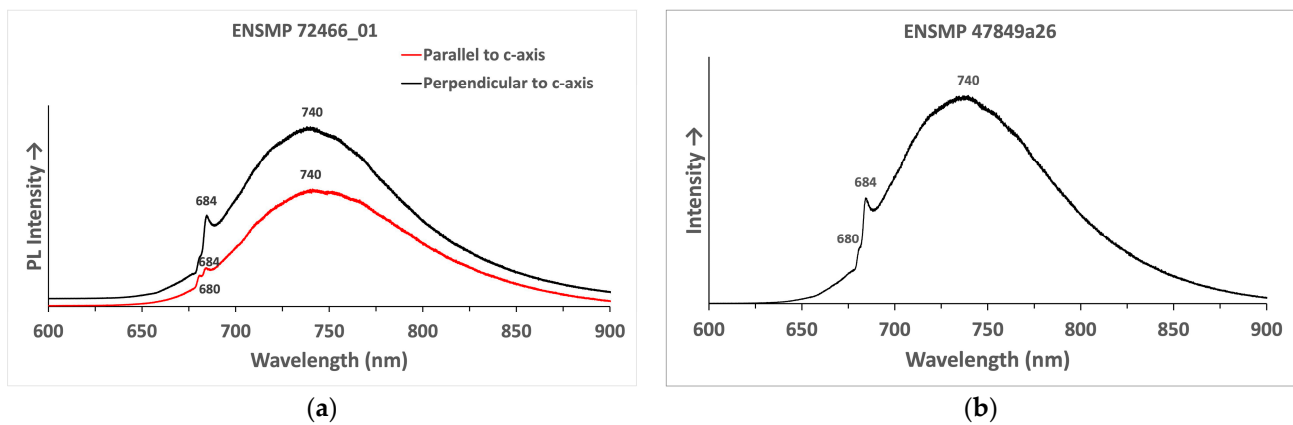


Figure 8. PL spectra of Egyptian emeralds (600–900 nm) from micro-Raman instrument. Sharp peaks near 680 nm are linked with Cr^{3+} . Broad band at 740 nm is also associated with the presence of Cr. (a) PL spectra of a single-crystal emerald (ENSMP 72466_01) parallel (red line) and perpendicular (black line) to c-axis. The upper spectrum has been vertically offset for better clarity. (b) PL spectra of an emerald from a sample, which is included in the host rock (ENSMP 47849a26).

3.4. FTIR Spectroscopy

Due to the irregular surface of the samples, we were not able to acquire FTIR spectra of good quality; in Figure 9, the FTIR spectrum of sample ENSMP 72466_01 is presented. Absorption bands at around 5273 cm^{-1} are linked to Type II water molecules [18]. Around 7095 cm^{-1} (i.e., ca. 1410 nm), a band related mainly to Type II water molecules is also observed with a relatively low signal vs. noise ratio [18,28]. Below 4000 cm^{-1} , the spectra were noisy due to sample surface.

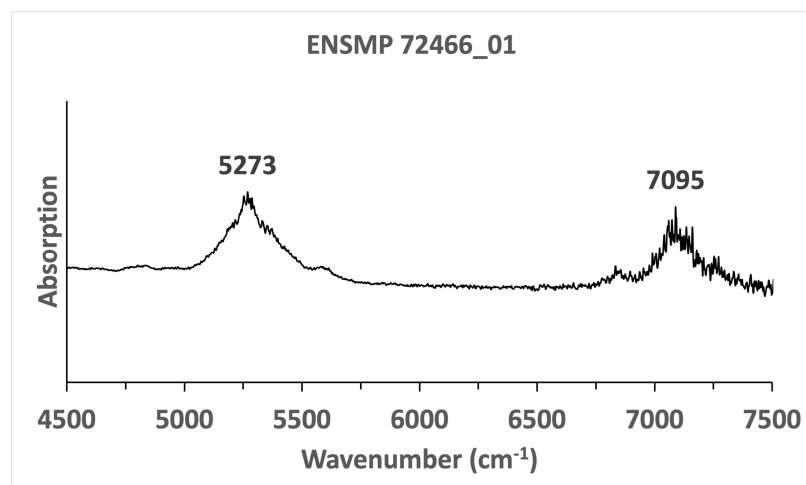


Figure 9. FTIR spectra of a single-crystal (ENSMP 72466_01) Egyptian emerald parallel to c-axis. The intense presence of peaks at 5273 cm^{-1} and 7095 cm^{-1} (about 1410 nm) are related to the presence of Type II water molecules.

3.5. UV-Vis-NIR Spectroscopy

The Egyptian emeralds studied here revealed absorption bands at around 430, 635 and 684 nm, which are mainly linked with Cr^{3+} [3,18,28,29] (Figure 10a,b) and a large band at around 840 nm is related to Fe^{2+} [3,28,29]. All studied samples presented similar absorption bands. In Vis-NIR spectra with the mobile spectrometer (Figure 10b), water-related bands at 960 nm were also observed [30]. An absorption band linked with Fe^{3+} in emeralds might be present at around 375–380 nm [3,18,28], but this cannot be confirmed in the acquired UV-Vis spectra (Figure 10a) due to samples' total absorption in the UV region.

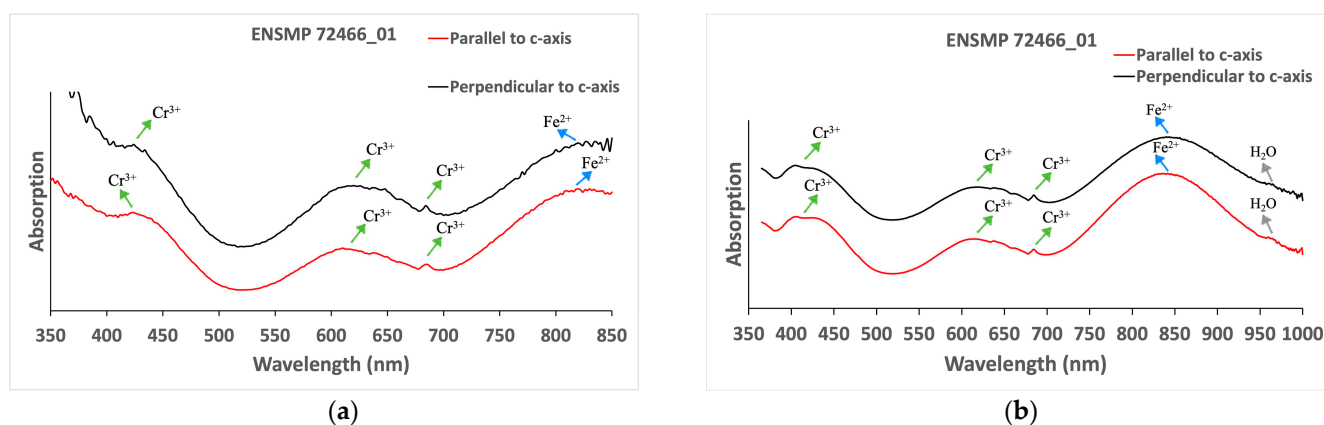


Figure 10. UV-Vis-NIR spectra of an Egyptian emerald single-crystal (ENSMP 72466_01). (a) UV-Vis spectra parallel (red line) and perpendicular (black line) to c-axis. The main chromophore elements are chromium and iron. (b) Vis-NIR spectra with the mobile instrument parallel (red line) and perpendicular (black line) to c-axis. Additional bands related to water molecules can also be observed at around 960 nm.

3.6. EDXRF

In our study, this method was applied in all samples except ENSMP 1352_5 due to its large size (Tables 3 and 4). All analyses are in ppmw, simply stated as ppm in this work. All samples revealed high concentrations of chromium and iron (up to 2315 and 19,795 ppm, respectively) but relatively low amounts of vanadium (below 665 ppm). Emerald crystals with bluish color (ENSMP 72466_03 and ENSM P72466-04) present higher concentrations of iron (Tables 3 and 4). Detectable amounts of Rb (11 to 84 ppm) were observed in all samples. In most cases, Cs was below the detection limit of the instrument (i.e., ca. 200 ppm) with one sample presenting a concentration slightly above 200 ppm but the chemistry is under the detection limits of the EDXRF instrument.

Table 3. Results of EDXRF analysis of single-crystal Egyptian emerald samples in ppm.

Samples	ENSMP 72466_01 (No. of Analysis: 3)		ENSMP 72466_02 (No. of Analysis: 4)		ENSMP 72466_03 (No. of Analysis: 4)		ENSMP 72466_04 (No. of Analysis: 3)	
	Min–Max Range	Average	Min–Max Range	Average	Min–Max Range	Average	Min–Max Range	Average
V ₂ O ₃	303–665	551.7	303–563	436	284–414	320.7	172–344	257.3
Cr ₂ O ₃	811–1202	1007.8	941–1735	1293.4	512–1000	715.8	1244–2228	1474.8
FeO	5018–13,348	7676.7	8909–14,057	11,700.3	8168–12,871	9797.3	10,577–19,791	16,233.7
Rb ₂ O	11–19	15.3	22–31	25	37–84	61	23–42	32.5

Table 4. Results of EDXRF analysis of Egyptian emerald crystals samples in host rock in ppm.

Samples	ENSMP 47849a26 (No. of Analysis: 3)		ENSMP 72486 (No. of Analysis: 3)		ENSMP 47849a27 (No. of Analysis: 1)
	Min–Max Range	Average	Min–Max Range	Average	Results
V ₂ O ₃	429–506	460	408–475	438	397.3
Cr ₂ O ₃	1568–2315	1935	1788–2120	1996	1873
FeO	2782–10,548	7296.7	11,277–12,052	11,710	7139
Rb ₂ O	25–53	36.6	48–63	54.3	10

3.7. Associated Minerals

Parts of the host rock were analyzed with micro-Raman technique in order to determine the minerals that take part in the paragenesis of the Egyptian emerald deposits. Micro-Raman spectroscopy revealed the presence of quartz, albite, phlogopite, calcite and dolomite. The peaks in quartz spectrum (Figure 11a) observed at 207 and 466 cm^{−1} are

due to symmetric stretching of Si-O while weaker bands located at 265, 355 and 809 cm^{-1} correspond to lattice modes and bending vibrations of Si-O, as well as a weak band at 1082 cm^{-1} that is related to the asymmetric stretching of SiO_4 [31–33].

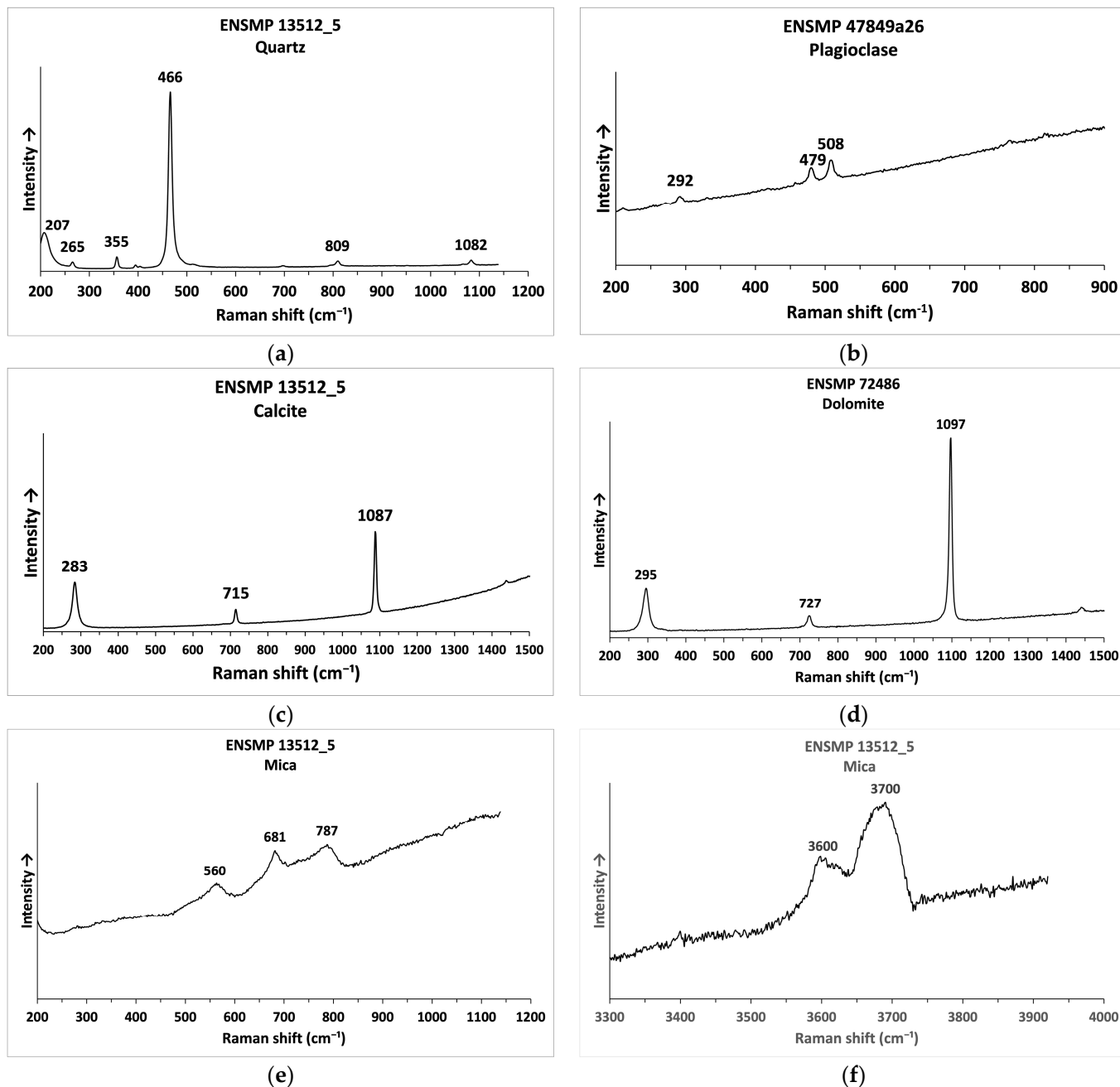


Figure 11. Micro-Raman spectra of minerals from the host rock of the Egyptian emeralds. (a) Raman spectra of quartz crystal (ENSMP 13512_5), (b) Raman spectra of plagioclase (ENSMP 47849a26), (c) Raman spectra of calcite (ENSMP 13512_5), (d) Raman spectra of dolomite (ENSMP 72486), (e,f) Raman spectra of mica (phlogopite) (ENSMP 13512_5).

Feldspar Raman bands (Figure 11b) correspond to plagioclase and possibly to albite with the Raman peaks at 292, 479 and 508 cm^{-1} related to SiO_4 ring vibrations [34,35]. Calcite and dolomite show Raman spectra (Figure 11 c,d) with the following peaks 295, 727 and 1097 cm^{-1} for dolomite and at 283, 715 and 1087 cm^{-1} for calcite due to different vibrations of carbonates [36,37]. The Raman spectrum on a mica inclusion (Figure 11e) shows the vibrations of phlogopite [34] with bands at 560, 681 and 787 cm^{-1} that correspond

to O3-T-O1 bend vibrations [35]. The Raman spectrum above 3500 cm^{-1} (Figure 11f) shows large bands at ca. 3600 and 3700 cm^{-1} , which are related to OH-stretching vibrations, possibly in phlogopite [36].

4. Discussion and Conclusions

Spectroscopic, chemical and gemological data on emeralds from Egypt are rare. This study presents such data on some historic rough emeralds from a museum collection, and it is part of a larger ongoing project on the study of historic gemmy material from the Mineralogy Museum of Mines Paris—PSL, in partnership with the LFG. Chemical analysis and spectra of all the studied emerald samples demonstrate similar features. Raman spectroscopy and FTIR spectra revealed that Type II water molecule vibrations, linked with alkali ions, are more intense than Type I water molecule vibrations. High alkali content is probably related with hydrothermal fluids derived from magmatic intrusions. All samples were colored by chromium and iron.

Using Raman spectra and under gemological microscope, the following were found as inclusions and associated minerals: growth tubes with rectangular-shaped multiphase fluid inclusions, quartz, feldspar (plagioclase, possibly albite), mica (likely phlogopite), calcite and dolomite. Quartz and albite are generally associated with granite or pegmatite intrusions and quartz veins, while phlogopite, calcite and dolomite are closely related with metamorphic zones between schists and pegmatite intrusions. All these inclusions and associated minerals are common in Egyptian emeralds [9] and are different from the inclusions in emeralds from other locations around the world, such as some of the very productive mines of gem quality samples in Zambia and Brazil [18,29].

Emerald is a mineral formed in moderate-to-high temperatures and is hosted by diverse rock types of different ages [2]. In our case, the main part of the emerald host rocks are pegmatite dikes with quartz, albite and phlogopite. Moderate Rb and low Cs concentrations were also observed and are probably associated with the S-type granite intrusions. Calcite and dolomite are secondary minerals in the metamorphic zone between the pegmatite quartz veins and the pre-existing schist rocks. Most of the Egyptian emerald deposits in Zabara area are found in the boundaries of these rocks next to the metamorphic zone [12,14].

Based on previous publications, emerald deposits can be classified in two main categories [2,14,37]. The first category is the Type I deposits, which are related with pegmatite or granite intrusions in rock sequences comprising the Archean or Precambrian basement. The second category are the Type II deposits in which the genesis of emeralds is relevant with tectonic events (mainly thrust faults and shear zones). The characterization of Egyptian emerald deposits seems to be doubtful according to the existing bibliography.

Recent studies classify these deposits as Type IID [2], which derive from metamorphic remobilization of Type I deposits. This theory states that initial Type I emerald deposits, which were related to hidden pegmatite or granite intrusions through mafic-ultramafic rocks (mostly amphibolites and schists) underwent later metamorphic and tectonic events that led to at least three generations of beryl crystals in Egypt [11]. Each emerald generation reflects an intense tectonic and metamorphic event [11]. These events are probably related with the presence of Na-plagioclase (low albite) by a metasomatic albitization event [14]. Additionally, the boudinage structure of the emeralds could be a result of extensional tectonic events. Some features, such as the quartz veins, may also be associated with later metamorphic events and the presence of S-type granites from the partial melting of preexisting sedimentary rocks [14]. The above results are consistent with the already existing recent studies; thus, Egyptian emeralds could be characterized as Type IID deposits and interpreted as a hybrid appearance of Type IA deposits that evolved into Type II deposits through tectonic and metamorphic events.

Emeralds have been used in jewelry pieces since the antiquity; however, their origin is still often debatable. It was suggested that emeralds from Hellenistic and Roman periods might be from Egypt, Pakistan and Afghanistan (also known as Bactrian emeralds), as well

as Russia (also known as Scythia) and Austria [38,39]. It is noteworthy that there is no written document or clear archaeological evidence of a link between Austrian emeralds and the Romans or Celts [40]. The present work will hopefully further contribute to the characterization of emeralds in the jewelry of archaeological significance.

Author Contributions: M.N. formulated the paper, prepared the experiments, performed data reduction, participated in the data interpretation, drew the figures and wrote the manuscript. S.K., E.G. and U.H. selected the samples, designed the experiments, performed some of the experiments, participated in the data interpretation and edited the manuscript. F.M., A.H., L.P., V.M., N.K., D.N. and A.D. participated in the data interpretation and edited the manuscript. All authors have read and agreed to the published version of the manuscript.

Funding: This research received no external funding.

Data Availability Statement: Not applicable.

Acknowledgments: The authors wish to thank all the colleagues at LFG and Museum of the Ecole des Mines, Mines Paris, PSL University, for their help during this study.

Conflicts of Interest: The authors declare no conflict of interest.

References

- Groat, L.A.; Giuliani, G.; Marshall, D.D.; Turner, D. Emerald Deposits and Occurrences; A Review. *Ore Geol. Rev.* **2008**, *34*, 87–112. [[CrossRef](#)]
- Giuliani, G.; Groat, L.A.; Marshall, D.; Fallick, A.E.; Branquet, Y. Emerald Deposits: A Review and Enhanced Classification. *Minerals* **2019**, *9*, 105. [[CrossRef](#)]
- Karampelas, S.; Al-Shaybani, B.; Mohamed, F.; Sangsawong, S.; Al-Alawi, A. Emeralds from the Most Important Occurrences: Chemical and Spectroscopic Data. *Minerals* **2019**, *9*, 561. [[CrossRef](#)]
- Sinkankas, J. *Emerald and Other Beryls*; Geoscience Press: Prescott, AZ, USA, 1981.
- Wood, D.L.; Nassau, K. The Characterization of Beryl and Emerald by Visible and Infrared Absorbance Spectroscopy. *Am. Mineral.* **1968**, *53*, 777–800.
- Huong, L.T.; Häger, W.; Hofmeister, W. Confocal Micro-Raman Spectroscopy: A Powerful Tool to Identify Natural and Synthetic Emeralds. *Gems Gemol.* **2010**, *64*, 36–41. [[CrossRef](#)]
- Wang, H.; Shu, T.; Chen, J.; Guo, Y. Characteristics of Channel-Water in Blue-Green Beryl and Its Influence on Colour. *Crystals* **2022**, *12*, 435. [[CrossRef](#)]
- Ogden, J. Cleopatra's Emerald Mines: The Marketing of a Myth. *J. Gemmol.* **2022**, *38*, 156–170. [[CrossRef](#)]
- Jennings, R.H.; Kammerling, R.C.; Kovaltchouk, A.; Calederon, G.P.; El Baz, M.K.; Koivula, J.I. Emeralds and Green Beryls of Upper Egypt. *Gems Gemol.* **1993**, *29*, 100–115. [[CrossRef](#)]
- Hume, W.F. *Geology of Egypt*; Government Press: Cairo, Egypt, 1934; Volume 2, p. 300.
- Giuliani, G. *Émeraude, Tout Un Monde*; Les Editions du Piat, Galvenas-F-43200: Saint-Julien-de-Pinet, France, 2022.
- Gawad, A.; Ene, A.; Skublov, S.G.; Gavrilchik, A.K.; Ali, M.A.; Ghoneim, M.M.; Nastavkin, A.V. Trace Element Geochemistry and Genesis of Beryl from Wadi Nugrus, South Eastern Desert, Egypt. *Minerals* **2022**, *12*, 206. [[CrossRef](#)]
- Soliman, M.M. Ancient Emerald Mines and Beryllium Mineralization Associated with Precambrian Stanniferous Granites in the Nugrus-Zabara Area, Southeastern Desert, Egypt. *Arab Gulf Res.* **1986**, *4*, 529–548.
- Grundmann, G.; Morteani, G. Multi-Stage Emerald Formation during Pan-African Regional Metamorphism: The Zabara, Sikait, Umm Kabo Deposits, South Eastern Desert of Egypt. *J. Afr. Earth Sci.* **2008**, *50*, 168–187. [[CrossRef](#)]
- Hassan, M.A.; El-Shatouri, H.M. Beryl Occurrences in Egypt. *Min. Geol.* **1976**, *26*, 253–262. [[CrossRef](#)]
- Gaillou, E.; Maouche, F.; Barthe, A.; Nectoux, D.; Lechartier, M. Émeraude Historiques de La Collection de l'École Nationale Supérieure Des Mines de Paris. *Le Règne Minéral* **2022**, *in press*.
- Cailliaud, F. *Voyage à l'Oasis de Thèbes et Dans Les Déserts Situés à l'Orient et à l'Occident de La Thébaïde (Histoire)*; Hachette Livre-BNF: Paris, France, 2022; ISBN 978-2-01-351722-5. (In French)
- Saeseaw, S.; Pardieu, V.; Sangsawong, S. Three-Phase Inclusions in Emerald and Their Impact on Origin Determination. *Gems Gemol.* **2014**, *50*, 114–132. [[CrossRef](#)]
- Jehlička, J.; Culka, A.; Bersani, D.; Vandabeele, P. Comparison of Seven Portable Raman Spectrometers: Beryl as a Case Study. *J. Raman Spectrosc.* **2017**, *48*, 1289–1299. [[CrossRef](#)]
- Bersani, D.; Azzi, G.; Lambruschi, E.; Barone, G.; Mazzoleni, P.; Raneri, S.; Longobardo, U.; Lottici, P.P. Characterization of Emeralds by Micro-Raman Spectroscopy. *J. Raman Spectrosc.* **2014**, *45*, 1293–1300. [[CrossRef](#)]
- Moroz, I.; Roth, M.; Boudeulle, M.; Panczer, G. Raman Microspectroscopy and Fluorescence of Emeralds from Various Deposits. *J. Raman Spectrosc.* **2000**, *31*, 485–490. [[CrossRef](#)]

22. Huong, L.T. Microscopic, Chemical and Spectroscopic Investigations on Emeralds of Various Origins. Ph.D. Thesis, Fachbereich Chemie, Pharmazie und Geowissenschaften der Johannes Gutenberg-Universität Mainz, Mainz, Germany, 2008.
23. Hagemann, H.; Lucken, A.; Bill, H.; Gysler-Sanz, J.; Stalder, H.A. Polarized Raman Spectra of Beryl and Bazzite. *Pgysiscs Chem. Miner.* **1990**, *17*, 395–401. [[CrossRef](#)]
24. Moroz, I.; Panczer, G.; Roth, M. Laser-Induced Luminescence of Emeralds from Different Sources. *J. Gemmol.* **1998**, *26*, 357–363. [[CrossRef](#)]
25. Huong, L.T.T.; Hofmeister, W.; Häger, T.; Karampelas, S.; Kien, N.D.T. A Preliminary Study on the Separation of Natural and Synthetic Emeralds Using Vibrational Spectroscopy. *Gems Gemol.* **2014**, *50*, 287–292. [[CrossRef](#)]
26. Wood, D.L. Absorption, Fluorescence, and Zeeman Effect in Emerald. *J. Chem. Phys.* **1965**, *42*, 3404–3410. [[CrossRef](#)]
27. Thompson, D.B.; Kidd, J.D.; Åström, M.; Scarani, A.; Smith, C.P. A Comparison of R-Line Photoluminescence of Emeralds from Different Origins. *J. Gemmol.* **2014**, *34*, 334–343. [[CrossRef](#)]
28. Mathieu, V.M. IR and UV-Vis Spectroscopy of Gem Emeralds, a Tool to Differentiate Natural, Synthetic and/or Treated Stones? Master's Thesis, Universiteit Gent, Ghent, Belgium, 2009.
29. Saeseaw, S.; Renfro, N.D.; Palke, A.C.; Sun, Z.; McClure, S.F. Geographic Origin Determination of Emerald. *Gems Gemol.* **2019**, *55*, 614–646. [[CrossRef](#)]
30. Araújo Neto, J.F.; Brito Barreto, S.; Carrino, T.A.; Müller, A.; Lira Santos, L.C.M. Mineralogical and Gemological Characterization of Emerald Crystals from Paraná Deposit, NE Brazil: A Study of Mineral Chemistry, Absorption and Reflectance Spectroscopy and Thermal Analysis. *Braz. J. Geol.* **2019**, *49*, 684–698. [[CrossRef](#)]
31. Buzgar, N.; Apopei, A.I.; Diaconu, V.; Buzatu, A. The Composition and Source of the Raw Material of Two Stone Axes of Late Bronze Age from Neamț County (Romania)—A Raman Study. *An. Stiintifice Ale Univ. "Al. I. Cuza" Din Iasi AUI Ser. Geol.* **2013**, *59*, 5–22.
32. Bersani, D.; Aliatis, I.; Tribaudino, M.; Mantovani, L.; Benisek, A.; Carpenter, M.A.; Gatta, G.D.; Lottici, P.P. Plagioclase Composition by Raman Spectroscopy. *J. Raman Spectrosc.* **2018**, *49*, 684–698. [[CrossRef](#)]
33. Sharma, S.K.; Misra, A.K.; Ismail, S.; Singh, U.N. Remote Raman Spectroscopy of Various Mixed and Composite Mineral Phases at 7.2 m Distance. In Proceedings of the 37th Lunar and Planetary Science Conference, League City, TX, USA, 13–17 March 2006.
34. Wang, A.; Freeman, J.; Jolliff, B.L. Understanding the Raman Spectral Features of Phyllosilicates. *J. Raman Spectrosc.* **2015**, *46*, 829–845. [[CrossRef](#)]
35. McKeown, D.A.; Bell, M.I.; Etz, E.S. Raman Spectra and Vibrational Analysis of the Trioctahedral Mica Phlogopite. *Am. Mineral.* **1999**, *84*, 970–976. [[CrossRef](#)]
36. Tlili, A.; Smith, D.C.; Beny, J.M.; Boyer, H. A Raman Microprobe Study of Natural Micas. *Mineral. Mag.* **1989**, *53*, 165–179. [[CrossRef](#)]
37. Schwarz, D.; Giuliani, G. Emerald Deposits-A Review. *Aust. Gemmol.* **2001**, *21*, 17–23.
38. Giuliani, G.; Chaussidon, M.; Schubnel, H.-J.; Piat, D.H.; Rollion-Bard, C.; Rance-Lanord, C.; Giard, D.; de Narvaez, D.; Rondeau, B. Oxygen Isotopes and Emerald Trade Routes Since Antiquity. *Science* **2000**, *287*, 631–633. [[CrossRef](#)] [[PubMed](#)]
39. Calligaro, T.; Dran, J.-C.; Poirot, J.-P.; Querre, G.; Salomon, J.; Zwaan, J.C. PIXE/PIGE Characterization of Emeralds Using an External Micro-Beam. *Nucl. Instrum. Methods Phys. Res. Sect. B Beam Interact. Mater. At.* **2000**, *161–163*, 769–774. [[CrossRef](#)]
40. Schmetzer, K. History of Emerald Mining in the Habachtal Deposit of Austria, Part II. *Gems Gemol.* **2022**, *58*, 18–46. [[CrossRef](#)]

Disclaimer/Publisher's Note: The statements, opinions and data contained in all publications are solely those of the individual author(s) and contributor(s) and not of MDPI and/or the editor(s). MDPI and/or the editor(s) disclaim responsibility for any injury to people or property resulting from any ideas, methods, instructions or products referred to in the content.